The protein kinase PknB negatively regulates biosynthesis and trafficking of mycolic acids in mycobacteria

Nguyen-Hung Le, Marie Locard-Paulet, Alexandre Stella, Nicolas Tomas, Virginie Molle, Odile Burlet-Schiltz, Mamadou Daffé, Hedia Marrakchi

PknB kinase regulates biosynthesis and trafficking of mycolic acids in mycobacteria

Nguyen-Hung Le[a§], Marie Locard-Paulet [a*], Alexandre Stella[a], Nicolas Tomas[a], Virginie Molle[b], Odile Burlet-Schiltz[a], Mamadou Daffé[a] and Hedia Marrakchi[a]#

[a]Institut de Pharmacologie et de Biologie Structurale, Université de Toulouse, CNRS, UPS, France

[b]Laboratoire de Dynamique des Interactions Membranaires Normales et Pathologiques, Université de Montpellier, CNRS, UMR 5235, Montpellier, France

Running title: Modulation of mycolic acid biogenesis by PknB

Corresponding author: Hedia Marrakchi

E-mail: hedia.marrakchi@ipbs.fr

§ Present address: Department of Molecular Microbiology, Washington University School of Medicine in St. Louis, MO.

*Present address: Novo Nordisk Foundation Center for Protein Research, University of Copenhagen. The center is supported financially by the Novo Nordisk Foundation (Grant agreement NNF14CC0001).

ABSTRACT

Mycobacterium tuberculosis, a causative agent of tuberculosis, remains one of the most wide-spread and deadliest pathogens in the world. A distinguishing feature of mycobacteria that sets them apart from other bacteria is the unique architecture of the cell wall characterized by the presence of various species-specific lipids, most notably mycolic acids (MAs). Therefore, targeted inhibition of enzymes involved in MA biosynthesis, transport and assembly has been extensively explored in drug discovery. Additionally, more recent evidence suggests that many enzymes in the MA biosynthesis pathway are regulated by kinase-mediated phosphorylation, thus opening additional drug development opportunities. However, how phosphorylation regulates mycolic acid production remains unclear. Here, we employed genetic strategies combined with lipidomics and phosphoproteomics approaches to investigate the role of phosphorylation in *Mycobacterium*. Our results revealed that PknB regulates export of MA and remodeling of the mycobacterial cell envelope. In particular, we identified the essential Mycobacterial membrane protein Large 3 (MmpL3) as a new substrate of PknB, thus directly linking kinase activity with MA trafficking. Taken together, our study documents the essential role of phosphorylation/dephosphorylation in regulating MA biosynthesis pathway and provides a blueprint for future anti-mycobacterial drug discovery.

Keywords: Mycobacteria, cell wall, mycolic acid, drug target, regulation, protein kinases, proteomics, phosphorylation, Fatty acid/Biosynthesis, lipids

INTRODUCTION

Mycobacterium tuberculosis (Mtu), a causative agent of tuberculosis (TB), remains one of the most wide-spread and deadliest pathogens in the world. Currently available treatment regimens for patients with active TB are significantly more complex than other bacterial infections and require the use of multiple antibiotics taken over the course of 6 to 9 months. The length, complexity and side effects of this chemotherapy may have contributed to the emergence of multi drug-resistant (MDR) and extensively drug-resistant (XDR) *Mtu* strains due to low compliance. This highlights the need for continued development of additional TB treatment options as well as further research into *Mtu* biological features that set it apart from other bacterial pathogens. One such distinguishing feature of mycobacteria is one-of-a-kind architecture of their cell wall, which provides a protective layer and renders the pathogen recalcitrant to chemical damage, dehydration and antibiotic treatment. This cell wall contains various species-specific lipids, most notably mycolic acids (MAs) that are unique to mycobacteria and play key roles in mycobacterial physiology and fitness (1) as well as in *Mtu* virulence and persistence within infected cells (2). MAs are very long-chain α-branched, β-hydroxylated fatty acids ranging from C_{70}-C_{90} (3). MAs represent the main constituents of the cell wall outer membrane (OM or mycomembrane) wherein they are anchored. MAs are transported across the plasma (inner) membrane as trehalose monomycolates (TMMs) and then are either covalently linked to the arabinogalactan-peptidoglycan to form the mycoloyl arabinogalactan peptidoglycan (mAGP) complex or incorporated into trehalose dimycolates (TDM), found in the outermost leaflet of the mycomembrane. The outer leaflet also contains other noncovalently associated lipids, such as phthiocerol dimycocerosates and sulfolipids (4).

MAs are synthesized in the cytoplasm via a highly conserved and well-characterized mixed fatty acid synthase (FAS)/polyketide synthase (PKS) biosynthetic pathway that has been extensively studied (5,6). Additionally, a molecular picture of cell-wall biogenesis process, which in *Mtu* involves 13 mycobacterial Membrane protein Large (MmpL) transporters that shuttle lipids across the membrane (7), has also emerged (8,9). However, intracellular regulation of cell wall biosynthesis still remains poorly

understood. Recently, phosphorylation mediated by Ser/Thr protein kinases (STPKs) has begun to emerge as a major regulation mechanism for many biological processes controlling mycobacterial infection and persistence (10-12). The *Mtu* genome encodes 11 STPKs named PknA, PknB and PknD-to-L. These enzymes are responsible for responding to environmental signals and coordinating cellular responses to ensure growth and survival. Recently, STPK-mediated phosphorylation has been reported to inhibit many enzymes involved in the MA biosynthesis, including proteins involved in MA chain elongation within the FAS-II system (13-16), mycolic chain modification (17), as well as the enzyme that specifically activates the meromycolic acid during mycolic condensation (18).

PknB is proposed to be one of the master regulators of Ser/Thr phosphorylation-mediated signaling in *Mtu* (19,20). It is essential and regulates the activity of a large repertoire of substrates, notably those involved in cell wall synthesis. Modulation of its expression levels has been shown to impact cellular morphology and survival (21,22), which suggests that the expression and activity of this kinase must be critically fine-tuned inside the bacterium. Its gene is localized in an operon containing two other essential genes involved in Ser/Thr phosphorylation: *pknA* and *pstP*. Interestingly, *pstP* is the only gene of *Mtu* known to encode a Ser/Thr phosphatase that likely forms a functional pair with PknB to control mycobacterial cell growth via modulating phosphorylation/dephosphorylation levels on substrate proteins (20,23). The dual regulation has only been reported for a few *Mtu* proteins, such as acyl-AMP ligase activity of FadD32 involved in the MA pathway (18). Despite these efforts, the full scope of STPK substrates remains unknown and the mechanistic and system-level link between intracellular phosphorylation/dephosphorylation events and cell wall biogenesis is not well understood. To begin to address this issue, we performed lipidomic and quantitative phosphoproteomic analysis of *M. smegmatis (Msm)* strains engineered to exhibit altered Ser/Thr phosphorylation through genetic manipulation. We depleted PstP to globally increase Ser/Thr phosphorylation levels, and combined with overexpression of *pknB* and its kinase-inactive mutant to identify PknB-dependent phosphorylations and their impact on cell wall composition and integrity through distinct

downstream changes in lipid profiles. We identify MmpL3 as the substrate of PknB, and this phosphorylation event as a major regulatory node in MA trafficking and cell wall biosynthesis.

MATERIALS AND METHODS

Plasmid construction. To produce PknB in *M. smegmatis* mc²155, the *pknB* gene was cloned into pLD1, an IPTG-inducible mycobacterial expression vector previously described (18). The *pknB* gene was PCR-amplified using a donor vector and primers (PknB_F and PknB_R, listed in Table S3) containing *Cla*I and *Nde*I restriction sites, respectively. To create the vector pLD1-*pknB*_K40M, the DNA portion of *pknB* containing the K40M mutation was transferred into pLD1-*pknB* using Gibson Assembly method. Briefly, fragment 1 was amplified from pLD1-*pknB* using the primers pair Frag1_F and Frag1_R, and fragment 2 was amplified from a donor vector using the primers pair Frag2_F and Frag2_R (Table S3). The 2 fragments were incubated together for 1h at 50°C using Gibson Assembly Master Mix (New England Biolab). *E. coli DH5α* competent cells were used to select successful assembly products. All the inserted sequences and mutation were confirmed by DNA sequencing (Eurofins Genomics, France).

Bacterial strains and culture conditions. The plasmids pLD1-null, pLD1-pknB and pLD1-pknB_K40M were electroporated into *M. smegmatis mc²155*. Transformants were selected on 7H10/0.05% Glycerol agar plates with Hygromycin B (100 µg/mL). Starter cultures were grown for 30h and then diluted in 7H9 medium (Difco) supplemented with Glycerol (2 g/L), Tyloxapol (0.025%) and Hygromycin B (100 µg/mL). The resulting cultures were incubated under shaking (180 RPM) at 37°C until reaching OD600 of 0.6. PknB overexpression was induced with IPTG (0.5 mM final) (Euromedex, France). Cells were harvested 4h after IPTG induction, washed with 50 mM PBS, pelleted by centrifugation, flash-frozen and kept at -80°C. Starter cultures of *M. smegmatis mc²-cd-pstP* were grown for 30h in 7H9 medium (Difco) supplemented with Glycerol (2 g/L), Tyloxapol (0.025%) and Kanamycin (50 µg/mL). Cultures were initiated at OD600 of 0,1 and grown in the absence or presence of anhydrotetracyclin (ATc) for 12h. The resulting cultures were

incubated under shaking (200 RPM) at 37°C until reaching an OD600 of 1. Cells were harvested, pelleted and kept at -80°C.

Immunoblotting. Cell pellets were thawed and resuspended in lysis buffer (50 mM HEPES pH7.5, 10% glycerol (v/v), 500 mM NaCl, and 2 mM 4-(2-Aminoethyl) benzenesulfonyl fluoride (AEBSF, Euromedex). The suspension was lysed with a cell disruptor (One Shot Model - Constant System Ltd., France) at 2.6 kbar. Total cell lysates were fractionated by SDS-PAGE, and then transferred to 0.4 µm Nitrocellulose membrane using the Transblot Turbo semi-dry transfer method (Biorad). Following the transfer, His-tagged PknB and PknB_K40M were detected using mouse monoclonal anti-polyHis antibodies (Sigma Aldrich) diluted 1/5000 or rat monoclonal anti-PknB antibodies (1652A rat antibody raised against the catalytic domain, gift from the STATENS SERUM INSTITUT); HRP-conjugated goat antibodies against mouse (Biorad, diluted 1/10000) or rat (Biorad, diluted 1/20000) were used as secondary antibodies. For *mc²-cd-pstP* cell pellets were thawed and resuspended in lysis buffer (50 mM Tris pH8, 8% glycerol (v/v), 500 mM NaCl, and 2 mM 4-(2-Aminoethyl) benzenesulfonyl fluoride (AEBSF, Euromedex). The suspension was lysed with a cell disruptor (One Shot Model - Constant System Ltd., France) at 2.6 kbar. Total cell lysates were fractionated by SDS-PAGE, and then transferred to 0.4 µm Nitrocellulose membrane using the Transblot Turbo semi-dry transfer method (Biorad). PstP-FLAG were detected using mouse monoclonal anti-FLAG antibodies HRP-conjugated (Sigma) diluted 1/10000. Detections were performed with Amersham^{Tm} ECL Prime Western Blotting Reagents Kit (GE Healthcare). Immunoreactive bands were revealed and measured with Chemidoc Imaging System (Biorad).

Lipid radiolabeling, extraction and analysis. To radiolabel all the lipids, 1,5 µL of [1-^{14}C] acetic acid (92,67x103 Bq, Amersham) were added to 5.4 mL of each *M. smegmatis* culture 3h post-induction. The cultures were incubated again for 1h at 37°C under shaking (150 RPM). Radiolabeled bacteria cultures were divided in two aliquots, and then harvested by centrifugation for 10 min at 2900 x g. Cell pellets were stored at -20°C.

To analyze labeled whole cell fatty acids, wet cell pellets were saponified with KOH (40%)/2-methoxyethanol (1/7; v/v) for 3 h at 110°C. FAs and MAs acids were extracted 3 times with diethyl ether and the resulting fractions acids were methylated using TMS-diazomethane (Sigma) and analyzed by thin layer chromatography (TLC) with CH_2Cl_2 as developing solvent.

The total extractable lipids (TEL) were obtained from wet bacterial pellets by two successive extractions using distinct mixtures of CHCl3/CH3OH (1/2 and 2/1, v/v). The fractions were pooled, washed with water, and dried. TLC bands of each radiolabeled lipid were quantified by PhosphorImaging and the ImageQuant software (Variable Mode Imager Typhoon TRIO, Amersham Biosciences). As reference, non-labeled lipid profiles were also analyzed.

For unlabeled lipid analysis, equivalent weights of total lipid fraction from each strain were spotted onto a HPTLC silica gel 60 plate (Merck) with a Camag ATS4 apparatus. The plates were developed in the indicated solvent system using a Camag ADC2 device and stained by immersion using a Camag CID3 apparatus with primuline (10% (w/v) in acetone/H2O 84/16) then revealed and quantified with Chemidoc Imaging System (Biorad).

Sample preparation for label-free proteomics and phosphoproteomics analysis. Flash-frozen cell pellets were resuspended in Urea lysis buffer (Urea 8 M, 50 mM Tris-HCl pH 8.0, Sodium Orthonovanadate 1 mM, supplemented with Complete Ultra tablets and Phosstop Phosphatase Inhibitor Cocktail tablets) and lysed with a cell disruptor (One Shot Model - Constant System Ltd., France) at 2.6 kbar. Non-lysed bacteria and cell debris were eliminated by centrifugation at 9000 x g. Protein concentrations of clarified lysates were quantified with Biorad DC Assay kit (Biorad). Equal amounts of lysate (3.1 mg) from each condition were reduced and alkylated with 5 mM Dithiothreitol (DTT) and 20 mM Iodoacetamide, respectively. Urea concentration was reduced to 1 mM by 8-fold dilution with Ammonium Bicarbonate 50 mM. The samples were then incubated overnight at 37°C with Trypsin at a ratio 1/100 (w/w, trypsin/proteins). After digestion, peptides were desalted using Sep-Pak columns (Waters; tC18 6cc 500 mg) following the provider instructions. Peptides were then dried down under vacuum and kept at -20°C.

Phospho-peptide enrichment. Titansphere TiO_2 beads (5 µm; GL Sciences 5020 75000) were pre-washed in TiO_2 loading buffer (80% MeCN, 5% Trifluoroacetic acid (TFA), 1 M glycolic acid). Peptide pellets (500 µg per sample) were suspended in TiO_2 loading buffer (1 µg/µL), and incubated with conditioned TiO_2 beads (6 mg of beads per mg of peptides) for 20 min under agitation at room temperature. Beads were then washed with washing buffer (60% acetonitrile 1% TFA) and loaded onto a home-made column (200 µL tip with an EMPORE C18 filter). Packed TiO_2 beads were washed once with washing buffer and phospho-peptides were eluted twice with 1% NH_4OH. Pooled eluates were acidified with TFA before being dried down under vacuum.

NanoLC-MS/MS Analysis. Peptides and phospho-peptides were analyzed by nanoLC-MS/MS using an UltiMate 3000 RSLCnano system (Dionex, Amsterdam, The Netherlands) coupled to a Q-ExactivePlus mass spectrometer (ThermoScientific, Bremen, Germany). Peptides were suspended in 5% acetonitrile, 0.05% TFA spiked with iRT (Biognosis 1X). 25% of each sample were loaded onto a C-18 precolumn (300-µm inner diameter x 5 mm, Dionex) at 20 µl/min in 5% acetonitrile, 0.05% TFA. After 5 min of desalting, the precolumn was switched online with the analytical C-18 column (75 µm inner diameter × 50 cm; in-house packed with Reprosil C18) equilibrated in 95% solvent A (5% acetonitrile, 0.2% formic acid) and 5% solvent B (80% acetonitrile, 0.2% formic acid). The peptides were eluted using a 4% to 40% gradient of solvent B at 300 nl/min flow rate for 240 min. The mass spectrometer was operated in data-dependent acquisition mode with the XCalibur software. Survey MS scans were acquired in the Orbitrap on the 400-1600 m/z range with a resolution of 70000, the 10 most intense ions per survey scan were selected for HCD fragmentation and resulting fragments were analyzed at a resolution of 17500 in the Orbitrap. The mass spectrometry proteomics data have been deposited to the ProteomeXchange (24) Consortium via the PRIDE (25) partner repository with the dataset identifier PXD012553.

Protein identification and quantification. Raw MS files were analyzed by MaxQuant version 1.5.5.1. Data were searched with the Andromeda search engine against *M. smegmatis* entries of the Swissprot protein database (strain ATCC 700084 / mc(2)155 Uniprot IDs UP000000757 and UP000006158 with 6602 and

6585 entries, respectively). In case of discrepancies in the residue numbering between the two combined databases of *Msm*, both phosphorylation site positions were reported, separated by the symbol "|". The search included methionine oxidation, serine, threonine and tyrosine phosphorylation as variable modifications, and carbamidomethylation of cysteine as a fixed modification. Validation was performed through a false discovery rate set to 1% at protein and peptide spectral match (PSM) level determined by target-decoy search in MaxQuant. Specificity of trypsin digestion was set for cleavage after lysine or arginine, and up to two missed cleavages were allowed. The precursor mass tolerance was set to 20 ppm for the first search and 4.5 ppm for the main Andromeda database search. The mass tolerance in MS/MS mode was set to 20 ppm. For label-free relative quantification of the samples, the "match between runs" option of MaxQuant was enabled to allow cross-assignment of MS features detected in the different runs.

Statistical analysis. The quantitative phosphoproteomic analysis was performed using the statistical package R (R Development Core Team, 2012; http://www.R-project.org/) and R scripts related to the analysis can be found online (https://github.com/mlocardpaulet/PhosphoSmegPKNB). Phosphorylation site relative quantification was performed with the intensities from the mono-phosphorylated peptides of the "Phospho (STY)" tables of MaxQuant with a localisation score $\geq 75\%$. Intensities were first normalized for instrument variation using spiked-in standards. Protein entries identified as potential contaminants by MaxQuant were eliminated from the analysis, as well as PSMs with a PEP value ≤ 0.01. Log2-transformed values of technical repeats were averaged. Each phosphorylation site relative quantities across the conditions were normalized to its cognate protein relative quantities determined by its LFQ values in the proteome (peptides analysis before phospho-enrichment). Then, missing values of the phosphorylation sites with < 1 data point across the 3 experiments were replaced for each condition (empty vector, PknB-K40M, PknB-WT) with the 1% quantile of the entire data set. In order to identify the PknB-dependent phosphorylation sites, we systematically performed two-sided unpaired Welch t-tests followed by Benjamini-Hochberg corrections of the p-value between the conditions. Phosphorylation sites were considered statistically

significant when they presented a corrected p-value ≤ 0.05 and a minimum absolute log2-transformed fold change ≥ 1 (corresponds to a two-fold change) (see Table S1 for the results of the statistical analysis).

Drug susceptibility testing. Colorimetric tetrazolium microplate assay was used to determine drug susceptibility of *M. smegmatis*. Non-frozen cell pellets from 30 mL cultures were vortexed with 2 mm glass beads and resuspended with 2 mL 7H9/0.02% Glycerol broth. The suspensions were then centrifuged at 100 x g to eliminate glass beads and bacterial clumps. The supernatants were used to prepare mycobacterial suspension at OD600 of 0.1. In a 96-well microplate (Nunc), 2 µL was added from two-fold dilution series of antibiotics in DMSO. For no inhibition control wells, 2 µL of DMSO was added instead. Next, 100 µL of 7H9/0.02% Glycerol broth was added into all wells, followed by 100 µL of mycobacteria suspension. The microplates were incubated at 37°C with moderate shaking (120 RPM). After 24h, 50 µL of Thiazolyl Blue Tetrazolium Bromide solution (Sigma) at 1 mg/mL was added to each well and re-incubated for 4h. In living bacteria, tetrazolium salts were reduced to insoluble formazan, which were solubilized by adding 50 µL of SDS 20%. When the formazan crystals were totally dissolved, absorbance at 570 nm was read with a microplate reader Clariostar (BMG Labtech, Germany). The inhibition curves (log10-transformed inhibitor concentration vs. Normalized response) were plotted using Graph Pad Prism 5.0.

RESULTS

The Msm Ser/Thr phosphatase PstP modulates cell envelope mycolates.

Given that PstP is the only known mycobacterial Ser/Thr protein phosphatase, we hypothesized that decrease of PstP activity would result in systemic perturbation of phosphorylation balance, and result in a phenotypic change in cell wall content. To test this hypothesis, we first examined the impact of PstP depletion on the different MA-containing lipids produced by *Msm*. We used a *Msm* mutant strain where the essential *pstP* gene was placed under the Tet-OFF promoter, which allowed us to induce PstP expression in the presence of anhydrotetracyclin (ATc) as described previously (26). The phosphatase depletion was confirmed by immunoblot (Fig. 1A). Following saponification of whole bacterial cells and lipid extraction, analysis of the resulting fatty acid (FA) and MA content showed no difference in their respective amounts between the wild-type ($PstP^+$) and PstP-depleted ($PstP^-$) strains (Table S1). However, when total bacterial lipids were solvent-extracted to yield the "total extractable lipid" fraction (triglycerides, glycopeptidolipids, phospholipids, trehalose-linked mycolic acids, etc.), we observed a significant (+90%) increase of the amount of TMM present in the $PstP^-$ strain compared to $PstP^+$ (Table S1, Fig. 1B and 1C). TMMs are the mycoloyl donors of the major mycolate-containing lipids of the mycomembrane (TDM and mycoloyl arabinogalactan-peptidoglycan). Thus, their increase notably impacts the TMM/TDM balance, with a ratio enhanced in the $PstP^-$ strain by 1.7 fold.

Our results show that PstP depletion is responsible for a significant increase of TMM abundance in *Msm*. This indicates that synthesis, transport or transfer of TMM may be regulated by phospho-Ser/Thr levels. Knowing that MA biosynthesis is regulated by Pkn kinase activities and given the essential and ubiquitous nature of PknB, we hypothesized that PknB could play a major role in MA metabolism, thereby participating in maintaining cell wall integrity. We decided to verify this hypothesis in a more controlled system through overexpression of PknB.

PknB plays a key role in maintaining cell envelope integrity.

To assess the role of PknB-mediated phosphorylation on the cell wall constituents, full length PknB from *Mtu* was overproduced with a N-terminal His-tag in *Msm*. As a control, we also expressed the mutant *Mtu pknB_K40M*, which is known to be enzymatically inactive (21). This ensured that the observed phenotypic differences between the strains expressing *pknB* or *pknB_K40M* were specific to PknB kinase activity, and not due to changes in protein quantity. The induction of *Mtu pknB* overexpression reduced *Msm* growth rate compared to wild type *Msm* or *Msm* expressing *Mtu pknB_K40M* 4h after induction (Fig. 2A, inset), which is in agreement with previously published data (22). We thus decided to perform all the experiments presented here (lipidomics, proteomics, drug sensitivity, etc) 4h following *pknB* variant induction. Indeed, at this time point the different strains have a similar growth rate, comparable biomass and total lipid/protein contents (Fig. 2), which allowed us to compare the phosphoproteomes and quantity of MA-containing lipids. Western blot analysis of the protein extracts from the different strains confirmed the overproduction of PknB and PknB_K40M (Fig. 2B), and their relative quantification by mass spectrometry indicated that they were expressed in similar amounts (Fig. S1).

In order to evaluate the possible impact of PknB kinase activity on the cell envelope integrity and/or remodeling, we compared the impact of large (rifampicin (RIF) and vancomycin (VAN)) compounds that enter the cells by diffusion through the lipid domain of the MM, and hydrophilic (isoniazid (INH) and ethambutol (EMB)) compounds that enter via pore-forming proteins (porins) (27,28), on the *Msm* strains expressing *pknB* or its inactive K40M mutant. Interestingly, the strain expressing *Mtu pknB* was specifically more sensitive to both large molecules, RIF (hydrophobic) and VAN (hydrophilic) (Fig. 2C, 2D), compared to the control and the mutant variant. This might be explained by a higher fluidity of the mycomembrane, permitting a better diffusion of the drugs. On the other hand, no significant change in the susceptibility to the small hydrophilic anti-TB drugs EMB and INH was measured in strains overexpressing PknB versus PknB_K40M. Altogether, these results indicate a measurable alteration of the cell wall properties resulting from induction of PknB kinase activity.

PknB activity regulates synthesis and transport of mycolic acids.

We hypothesized that the increase of *Msm* sensitivity to RIF and VAN upon induction of PknB kinase activity could result from an alteration of the cell envelope composition. To investigate the impact of PknB kinase activity on FA and MA content, bacteria were harvested after induction of the *pknB* variants expression. In order to monitor MA production, and improve the sensitivity of detection of fine changes in metabolism, cells were harvested 3h post-induction and labelled with ^{14}C-acetate for 1h. Whole bacterial cells were either saponified (to obtain total MAs and FAs) (Fig. 3A), or extracted with organic solvents ($CHCl_3$/CH_3OH) to yield total non-covalently linked extractable lipids (TEL) (Fig. 3B). Samples were then resolved and detected by radio-thin layer chromatography (Fig. 3; Table S2). The incorporation of labelled acetate into total FAs and MAs dramatically decreased in *Msm* overexepressing *Mtu PknB* (-34% and -60%, respectively), compared to the control strain harboring the empty vector and the strain expressing the inactive K40M isoform. Thus, MA production was reduced upon induction of PknB kinase activity. In parallel, in the non-covalently linked (organic solvent-extracted) lipids, mycolates in the form of TMMs notably accumulated (+42%) while TDM quantities significantly decreased (-58%) (Fig. 3B; Table S2) in the PknB-overexpression strain. Previously, this imbalance of TMM/TDM ratio in favor of TMM (>3-fold increase) was observed upon inhibition of MmpL3, either using small molecule inhibitors (29,30) or in conditional mycobacterial *mmpL3* mutants (31). Interestingly, triglyceride quantification showed no difference in the incorporation of radioactivity between the three strains (Fig. S2), whereas incorporation of radioactivity into FAs, precursors of phospholipids and MA chains, also decreased (Fig. S2 and Table S2). Taken together, our data suggest that PknB kinase activity impacts not only FA and MA synthesis, but the transport of MAs to the cell wall as well, an insight that has not been documented before.

PknB kinase overexpression identifies proteins of the cell envelope as major substrates

To explore the possibility that PknB affects MA transport via direct phosphorylation of protein(s) involved in this process, we performed a large-scale quantitative phoshophoproteomic analysis of the different *Msm* strains. Three independent cultures of *Msm* transformed with empty vector, *pknB* and *pknB_K40M* were

prepared. Bacteria were lysed, proteins were trypsin-digested and phosphorylated peptides were then enriched using titanium dioxide beads. Peptides before and after phospho-enrichment were analyzed by liquid chromatography coupled to tandem mass spectrometry (LC-MS/MS) to determine relative abundance of protein and phosphorylation sites across samples, respectively (Fig. 4A). We then performed two-sided unpaired t-tests followed by a Benjamini-Hotchberg correction of the *p*-values to determine the proteins and phosphorylation sites regulated upon induction of PknB kinase activity. We identified four times as many phosphorylation sites upon *Mtu* PknB overproduction compared to both controls (Fig. S3 panel A). The phosphorylation sites quantified in both control conditions exhibited similar relative abundance, as expected (Fig. S3 panel B). Kinase activity of *Mtu* PknB increased both the number of phosphorylated sites and their intensity in *Msm*, as all phosphopeptides detected upon induction of *Mtu* PknB were more abundant than in any of the control conditions (Fig. S3 panels C and D).

Interestingly, while phosphoproteomics data indicate a systems-wide increase in phosphorylation upon induction of PknB activity, less than 1% of the *Msm* proteome was significantly altered upon expression of *Mtu* PknB compared to the controls (Dataset S1). This suggests that the differences observed between the three strains are more likely due to the phosphorylation status of protein substrates, rather than to differences in protein expression.

Moreover, number and nature of significantly regulated phosphorylation sites (Fig. S3 panel E) indicate prevalence of phospho-threonines over phospho-serines and phospho-tyrosines, which is in agreement with the reported “bias” of mycobacterial STPK towards threonines (32).

Our analysis identified 2256 phosphorylation sites on 1194 proteins (Dataset S1), amongst which 1385 phosphorylation sites (from 811 proteins) were differentially regulated between the strains displaying enhanced PknB kinase activity compared to the inactive PknB_K40M (Fig. S3A). Differentially regulated sites were identified on proteins known to be regulated by PknB, such as PknB itself, GarA (a FHA domain-containing protein), PtsP (Ppp) and Wag31 (DivIVA), an essential protein organizing cell wall biosynthesis at the growing cellular poles (11) (Fig. S4). In addition to confirming results from previous studies (32,33), we identified a significant number of previously unreported phosphorylated proteins in the MA pathway,

thus expanding the mycobacterial phosphoproteome. Notably, we document that threonine 22 (T22) on *de novo* fatty acid synthase FAS-I displayed differential PknB activity-dependent phosphorylation, as well as proteins involved in the biosynthetic pathway of MAs: dehydratase HadA, β-ketoacyl-ACP reductase MabA (FabG), acyl-CoA carboxylase subunits AccA3 (T533) and AccD5 (T2, S8 and T29), and the mycolic condensing enzyme Pks13 (T14, T1445, T1450) (Fig. 4B). Some of our data recapitulates previously reported link between PknB activity on substrates such as adenylating enzyme FadD32 and Pks13 (Fig. 4B; (32,34). Moreover, we also describe sites which were not previously known to be subject to PknB phosphorylation such as those on ACCases.

Importantly, among the highly regulated phosphorylation sites, we identified threonine 984 (T984) on MmpL3, further supporting the proposed role of PknB activity in regulation of MA trafficking (Fig. 4B). Collectively, our lipidomic and phosphoproteomic analyses reveal that PknB plays a global regulatory role, not only on the production of MAs, but on their export to the mycomembrane as well, thus participating in the remodeling of the cell envelope (Fig. 5).

DISCUSSION

Mycobacterial STPKs have emerged as critical regulators of viability and survival, for example by phosphorylating substrate proteins involved in MA biosynthesis known to be critical for *Mtu* cell wall adaptation. Such mechanisms rely on a tight and reversible balance of Ser/Thr phosphorylation/dephosphorylation. In *Mtu*, and closely related *Msm*, PknB is one of the best characterized kinases that is central for regulation of mycobacterial signaling, although additional kinases are relevant as well given that *Mtu* genome codes for 11 STPKs, while PstP is the only phosphatase identified to date. Therefore, the interplay between PknB and PstP activities is expected to be critically important for mycobacterial physiology. While we were preparing this work, two independent studies characterizing PstP were published, both suggesting that this phosphatase plays a central role in regulating cell division (26,35), as well as cell wall biosynthesis and global phosphorylation levels (35). Here, we provide more granular evidence that PstP plays an important role in regulating MA biosynthesis based on the observation that PstP depletion significantly increased the quantities of TMM, a precursor for mycolic acids.

To further investigate this phenotype, we produced the ubiquitous and essential protein kinase PknB from *Mtu* and its enzymatically inactive K40M mutant in *Msm*, to study the importance of PknB-dependent phosphorylation in regulating the MA metabolism. Although induction of *Mtu PknB* overexpression had little impact on the *Msm* proteome, it caused a major change in the permeability of the cells to the large-size drugs RIF and VAN, indicating remodeling of the envelope. As expected (22), a specific reduction of the growth rate of *pknB*-expressing *Msm* was observed after 4h of induction. Accordingly, labeling of bacterial cells with ^{14}C-acetate following PknB-induction showed a drastic decrease of MA synthesis and a specific and dramatic change in the balance of trehalose mycolates in the overexpressing strain. An accumulation of TMM was observed, with a decrease of the quantities of TDM, the final acceptor of MAs. These observations were dependent on the kinase activity of PknB since no effect was observed in *Msm* overexpressing the inactive K40M mutant, and comparable to those obtained upon inhibition of trehalose monomycolate transport from the cytosol to the cell wall by MmpL3.

Consistently, a comparative analysis of the phosphoproteomes of these mycobacterial strains demonstrated the phosphorylation of several proteins involved in both the synthesis and transport of MAs, especially MmpL3 (Fig. 4). In fact, phosphorylation of MmpL3 pheno-copied both mycobacterial depletion of this protein and inhibition of the cell wall lipid TMM export by MmpL3 inhibitors. This identifies for the first time the negative modulation of MmpL3 activity by STPK-regulation, and adds MmpL3 as a new "piece" in the landscape of cell wall biogenesis proteins negatively-regulated by STPK phosphorylation (36) (Fig. 5).

Altogether, our results not only confirm previously known PknB-dependent phosphorylation sites on proteins involved in MA biosynthesis, but also identified new phosphorylated proteins involved in MA biosynthesis and trafficking, thus expanding the mycobacterial phosphoproteome. These data brought to light the phospho-dependent regulation of *Msm* cell envelope integrity through regulation of enzymes involved in FA and MA metabolism (Fig 4B). These findings support a working model in which phosphorylation of FAS-II enzymes reduce the production of MAs, which transport by MmpL3 is in turn negatively regulated by phosphorylation, thus generating the accumulation of TMM and the reduction of their final acceptors, *i.e.* TDM and cell-wall arabinogalactan (Fig. 5).

Cell envelope biogenesis —and in particular MA synthesis— is a validated pathway for anti-TB drug discovery. The present study provides a set of phosphorylation sites that are under control of PknB kinase activity. These include known PknB substrates (FadD32, HadA, MabA), as well as new sites potentially involved in drug resistance and adaptation to the host (20,37). These data, together with our lipidomics analysis of cell wall remodeling upon Ser/Thr phosphorylation, indicate that cell wall biogenesis relies on phosphorylation of proteins involved in MA synthesis and transport, including MmpL3, an essential mycolate transporter and the proposed target of many anti-mycobacterial inhibitors under development (29-31,38). These findings are in line with a recent study pointing to mycobacterial cell envelope lipid alteration and the decreased phosphorylation of MmpL3 upon treatment with PknA and PknB inhibitors (39). Overall, these data highlight the critical role of MA regulation by STPKs and, as such,

confirm that phospho-regulation of the essential cell wall metabolism represents a promising target for anti-mycobacterial drug discovery.

DATA AVAILABILITY STATEMENT

All the data described are contained within this manuscript.

ACKNOWLEDGEMENTS/GRANT SUPPORT

We are grateful to Dr Vinay Nandicoori for his gift of the *M. smegmatis pstP* strain. N.L. was supported by a fellowship from the French Foreign Office (Ministère des Affaires Etrangères). We acknowledge funding from the Agence Nationale de la Recherche (FASMY, grant ANR-14-CE16-0012). For O.B-S., this work was supported in part by the Région Midi-Pyrénées, European funds (Fonds Européens de Développement Régional, FEDER), Toulouse Métropole, and the French Ministry of Research with the Investissement d'Avenir Infrastructures Nationales en Biologie et Santé program (ProFI, Proteomics French Infrastructure project, ANR-10-INBS-08).

AUTHOR CONTRIBUTIONS

HL, MD and HM designed the project; HL, MLP, NT, AS, HM designed and performed experiments and analyzed the data, HL, MLP, NT and HM prepared the figures. HL, VM, MLP, MD and HM wrote the manuscript. All authors reviewed the manuscript.

CONFLICT OF INTEREST

The authors declare that they have no conflicts of interest with the contents of this article.

REFERENCES

1. Jamet, S., Slama, N., Domingues, J., Laval, F., Texier, P., Eynard, N., Quémard, A., Peixoto, A., Lemassu, A., Daffé, M., and Cam, K. (2015) *PloS one* **10**
2. Verschoor, J. A., Baird, M. S., and Grooten, J. (2012) *Progress in lipid research* **51**, 325-339
3. Daffé M., Q. A., Marrakchi H. . (2017) Mycolic Acids: From Chemistry to Biology. in *Biogenesis of Fatty Acids, Lipids and Membranes.* (O., G. ed.), Springer, Cham. pp
4. Daffé, M., and Marrakchi, H. (2019) *Microbiology spectrum* **7**
5. Marrakchi, H., Lanéelle, M.-A. A., and Daffé, M. (2014) *Chemistry & biology* **21**, 67-85
6. Quémard, A. (2016) *Trends in microbiology* **24**, 725-738
7. Chalut, C. (2016) *Tuberculosis (Edinburgh, Scotland)* **100**, 32-45
8. Varela, C., Rittmann, D., Singh, A., Krumbach, K., Bhatt, K., Eggeling, L., Besra, G. S., and Bhatt, A. (2012) *Chemistry & biology* **19**, 498-506
9. Xu, Z., Meshcheryakov, V. A., Poce, G., and Chng, S.-S. S. (2017) *Proceedings of the National Academy of Sciences of the United States of America* **114**, 7993-7998
10. Wehenkel, A., Bellinzoni, M., Graña, M., Duran, R., Villarino, A., Fernandez, P., Andre-Leroux, G., England, P., Takiff, H., Cerveñansky, C., Cole, S. T., and Alzari, P. M. (2008) *Biochimica et biophysica acta* **1784**, 193-202
11. Richard-Greenblatt, M., and Av-Gay, Y. (2017) *Microbiology spectrum* **5**
12. Av-Gay, Y., and Everett, M. (2000) *Trends in microbiology* **8**, 238-244
13. Molle, V., Brown, A. K., Besra, G. S., Cozzone, A. J., and Kremer, L. (2006) *The Journal of biological chemistry* **281**, 30094-30103
14. Slama, N., Leiba, J., Eynard, N., Daffé, M., Kremer, L., Quémard, A., and Molle, V. (2011) *Biochemical and biophysical research communications* **412**, 401-406
15. Veyron-Churlet, R., Molle, V., Taylor, R. C., Brown, A. K., Besra, G. S., Zanella-Cléon, I., Fütterer, K., and Kremer, L. (2009) *The Journal of biological chemistry* **284**, 6414-6424

16. Vilchèze, C., Molle, V., Carrère-Kremer, S., Leiba, J., Mourey, L., Shenai, S., Baronian, G., Tufariello, J., Hartman, T., Veyron-Churlet, R., Trivelli, X., Tiwari, S., Weinrick, B., Alland, D., Guérardel, Y., Jacobs, W. R., and Kremer, L. (2014) *PLoS pathogens* **10**

17. Corrales, R. M., Molle, V., Leiba, J., Mourey, L., de Chastellier, C., and Kremer, L. (2012) *The Journal of biological chemistry* **287**, 26187-26199

18. Le, N.-H. H., Molle, V., Eynard, N., Miras, M., Stella, A., Bardou, F., Galandrin, S., Guillet, V., André-Leroux, G., Bellinzoni, M., Alzari, P., Mourey, L., Burlet-Schiltz, O., Daffé, M., and Marrakchi, H. (2016) *The Journal of biological chemistry* **291**, 22793-22805

19. Baer, C. E., Iavarone, A. T., Alber, T., and Sassetti, C. M. (2014) *The Journal of biological chemistry* **289**, 20422-20433

20. Kaur, P., Rausch, M., Malakar, B., Watson, U., Damle, N. P., Chawla, Y., Srinivasan, S., Sharma, K., Schneider, T., Jhingan, G. D., Saini, D., Mohanty, D., Grein, F., and Nandicoori, V. K. (2019) *Nature communications* **10**, 1231

21. Chawla, Y., Upadhyay, S., Khan, S., Nagarajan, S. N., Forti, F., and Nandicoori, V. K. (2014) *The Journal of biological chemistry* **289**, 13858-13875

22. Kang, C.-M. M., Abbott, D. W., Park, S. T., Dascher, C. C., Cantley, L. C., and Husson, R. N. (2005) *Genes & development* **19**, 1692-1704

23. Boitel, B., Ortiz-Lombardía, M., Durán, R., Pompeo, F., Cole, S. T., Cerveñansky, C., and Alzari, P. M. (2003) *Molecular microbiology* **49**, 1493-1508

24. Deutsch E.W., C. A., Sun Z., Jarnuczak A., Perez-Riverol Y., Ternent T., Campbell D.S., Bernal-Llinares M., Okuda S., Kawano S., Moritz R.L., Carver J.J., Wang M., Ishihama Y., Bandeira N., Hermjakob H., Vizcaíno J.A. (2017) *Nucleic acids research* **54(D1)**, D1100-D1106

25. Perez-Riverol, Y., Csordas, A., Bai, J., Bernal-Llinares, M., Hewapathirana, S., Kundu, D. J., Inuganti, A., Griss, J., Mayer, G., Eisenacher, M., Perez, E., Uszkoreit, J., Pfeuffer, J., Sachsenberg, T., Yilmaz, S., Tiwary, S., Cox, J., Audain, E., Walzer, M., Jarnuczak, A. F., Ternent, T., Brazma, A., and Vizcaino, J. A. (2019) *Nucleic Acids Res* **47**, D442-D450

26. Sharma, A. K., Arora, D., Singh, L. K., Gangwal, A., Sajid, A., Molle, V., Singh, Y., and Nandicoori, V. K. (2016) *The Journal of biological chemistry* **291**, 24215-24230

27. Brennan, P. J., and Nikaido, H. (1995) *Annual review of biochemistry* **64**, 29-63

28. Stahl, C., Kubetzko, S., Kaps, I., Seeber, S., Engelhardt, H., and Niederweis, M. (2001) *Molecular microbiology* **40**, 451-464

29. Grzegorzewicz, A. E., Pham, H., Gundi, V. A., Scherman, M. S., North, E. J., Hess, T., Jones, V., Gruppo, V., Born, S. E., Korduláková, J., Chavadi, S. S., Morisseau, C., Lenaerts, A. J., Lee, R. E., McNeil, M. R., and Jackson, M. (2012) *Nature chemical biology* **8**, 334-341

30. Tahlan, K., Wilson, R., Kastrinsky, D. B., Arora, K., Nair, V., Fischer, E., Barnes, S. W., Walker, J. R., Alland, D., Barry, C. E., and Boshoff, H. I. (2012) *Antimicrobial agents and chemotherapy* **56**, 1797-1809

31. Li, W., Obregon-Henao, A., Wallach, J. B., North, E. J., Lee, R. E., Gonzalez-Juarrero, M., Schnappinger, D., and Jackson, M. (2016) *Antimicrob Agents Chemother* **60**, 5198-5207

32. Prisic, S., Dankwa, S., Schwartz, D., Chou, M. F., Locasale, J. W., Kang, C.-M. M., Bemis, G., Church, G. M., Steen, H., and Husson, R. N. (2010) *Proceedings of the National Academy of Sciences of the United States of America* **107**, 7521-7526

33. Fortuin, S., Tomazella, G. G., Nagaraj, N., Sampson, S. L., Gey van Pittius, N. C., Soares, N. C., Wiker, H. G., de Souza, G. A., and Warren, R. M. (2015) *Front Microbiol* **6**

34. Le, N. H., Molle, V., Eynard, N., Miras, M., Stella, A., Bardou, F., Galandrin, S., Guillet, V., Andre-Leroux, G., Bellinzoni, M., Alzari, P., Mourey, L., Burlet-Schiltz, O., Daffe, M., and Marrakchi, H. (2016) *J Biol Chem* **291**, 22793-22805

35. Iswahyudi, Mukamolova, G. V., Straatman-Iwanowska, A. A., Allcock, N., Ajuh, P., Turapov, O., and O'Hare, H. M. (2019) *Scientific reports* **9**, 8337

36. Molle, V., and Kremer, L. (2010) *Mol Microbiol* **75**, 1064-1077

37. Baros, S. S., Blackburn, J. M., and Da Cruz Soares, N. A. (2019) *Molecular & cellular proteomics : MCP*

38. Li, W., Upadhyay, A., Fontes, F. L., North, E. J., Wang, Y., Crans, D. C., Grzegorzewicz, A. E., Jones, V., Franzblau, S. G., Lee, R. E., Crick, D. C., and Jackson, M. (2014) *Antimicrobial agents and chemotherapy* **58**, 6413-6423

39. Carette, X., Platig, J., Young, D. C., Helmel, M., Young, A. T., Wang, Z., Potluri, L. P., Moody, C. S., Zeng, J., Prisic, S., Paulson, J. N., Muntel, J., Madduri, A. V. R., Velarde, J., Mayfield, J. A., Locher, C., Wang, T., Quackenbush, J., Rhee, K. Y., Moody, D. B., Steen, H., and Husson, R. N. (2018) *mBio* **9**

Figure 1

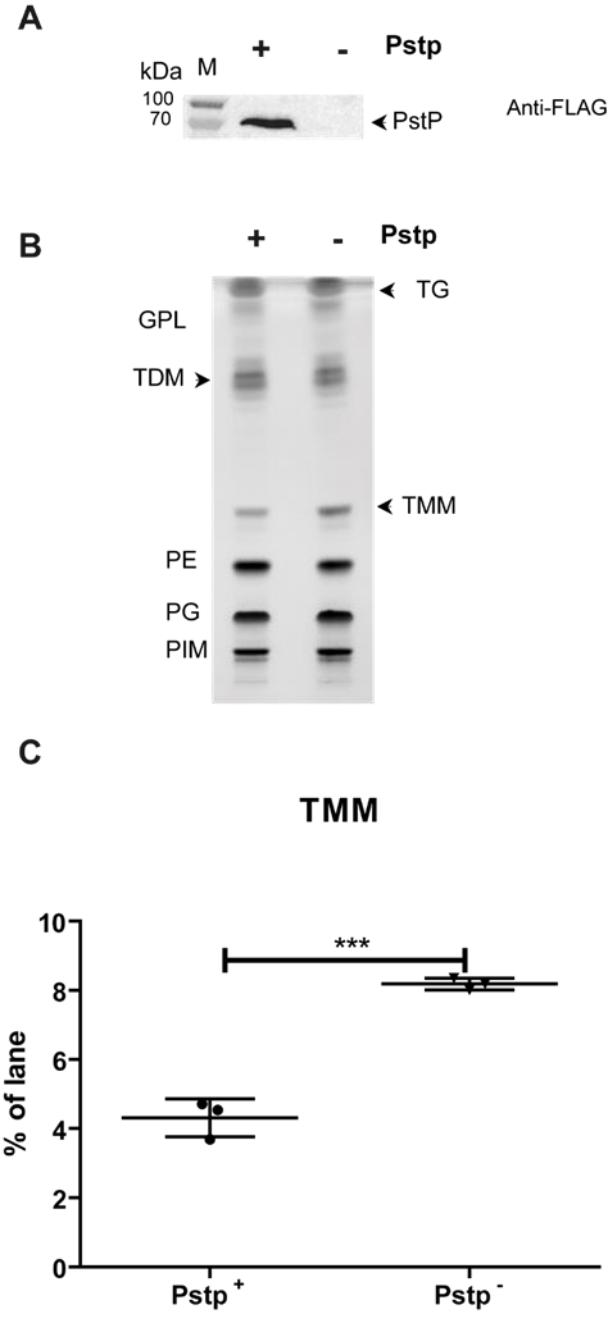
A
+
-
Pstp
kDa
M
100
70
PstP
Anti-FLAG
B
+
-
Pstp
TG
GPL
TDM
TMM
PE
PG
PIM
C
TMM
***
10
8
6
4
2
0
% of lane
Pstp +
Pstp -

Figure 2

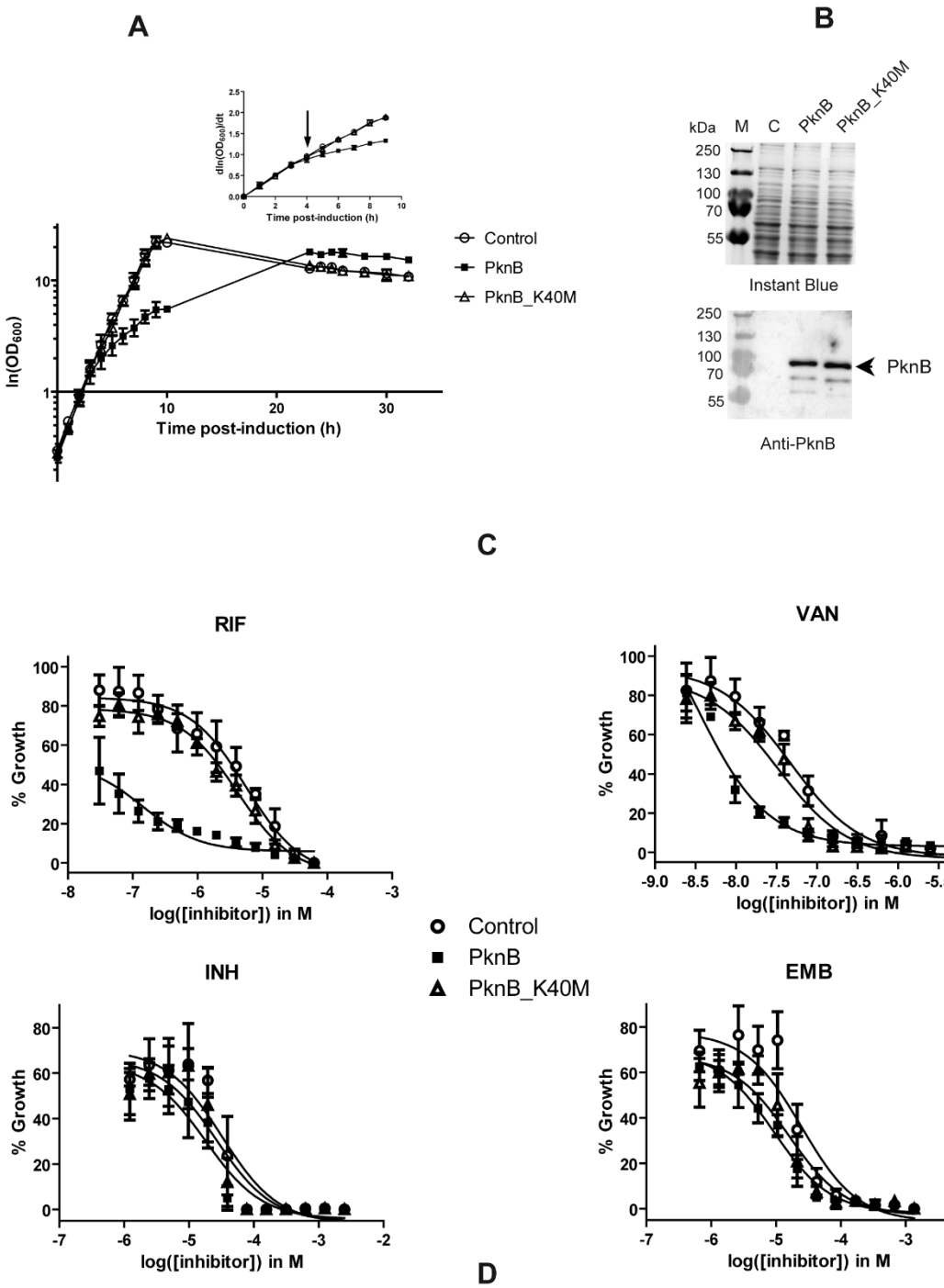

D

	IC50 (µM)			
	RIF	**VAN**	**INH**	**EMB**
Control	5,35 ± 2,47	0,050 ± 0,017	33,28 ± 7,05	26,06 ± 11,87
PknB	0,30 ± 0,30	0,003 ± 0,002	17,77 ± 5,35	9,30 ± 0,66
PknB_K40M	4,24 ± 1,29	0,029 ± 0,014	29,38 ± 14,21	17,32 ± 9,33

Figure 3

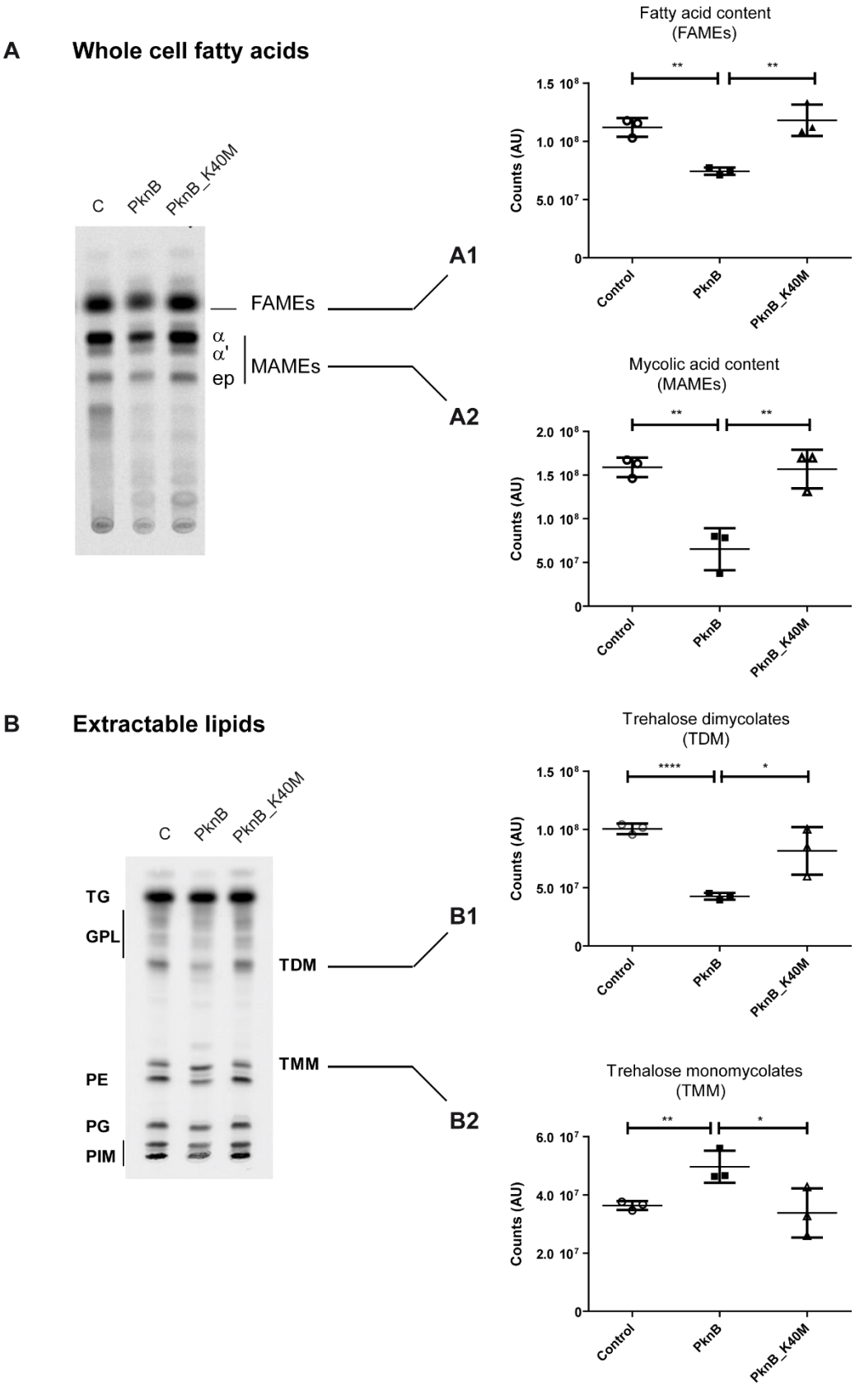
A
Whole cell fatty acids
C
PknB
PknB_K40M
FAMEs
α
α'
ep
MAMEs
A1
A2
Fatty acid content
(FAMEs)
Mycolic acid content
(MAMEs)
Counts (AU)
Control
PknB
PknB_K40M
B
Extractable lipids
TG
GPL
PE
PG
PIM
TDM
TMM
B1
B2
Trehalose dimycolates
(TDM)
Trehalose monomycolates
(TMM)

Figure 4

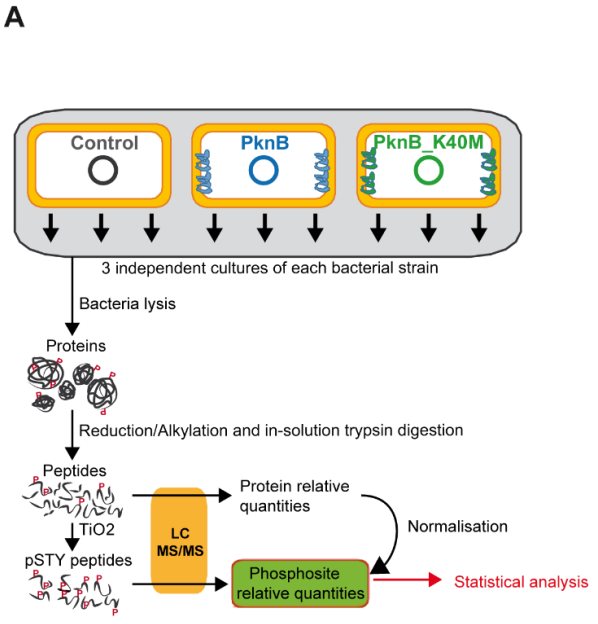
A
Control
PknB
PknB_K40M
3 independent cultures of each bacterial strain
Bacteria lysis
Proteins
Reduction/Alkylation and in-solution trypsin digestion
Peptides
TiO2
pSTY peptides
LC MS/MS
Protein relative quantities
Phosphosite relative quantities
Normalisation
Statistical analysis

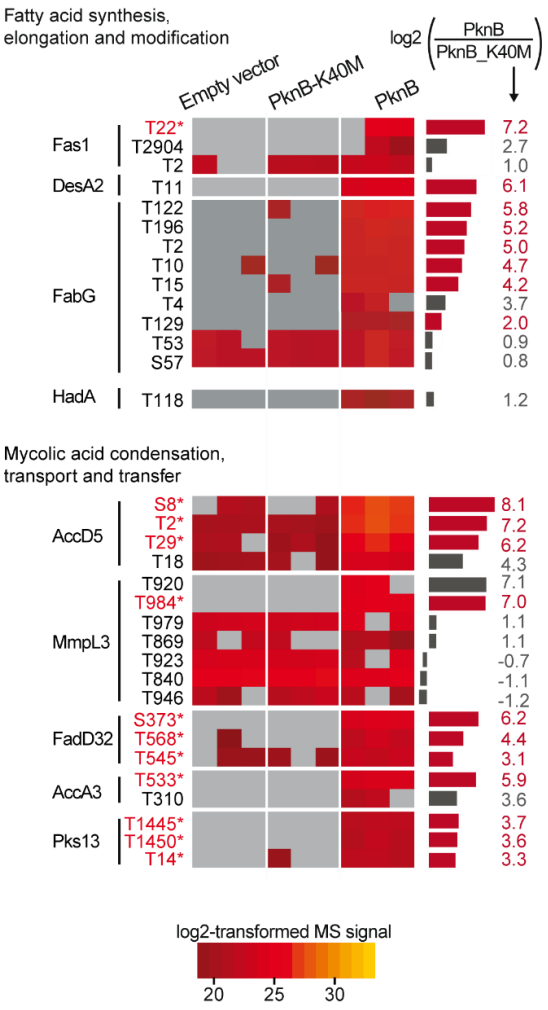
B
Fatty acid synthesis, elongation and modification
log2 (PknB / PknB_K40M)
Empty vector
PknB-K40M
PknB
Fas1
T22* 7.2
T2904 2.7
T2 1.0
DesA2
T11 6.1
FabG
T122 5.8
T196 5.2
T2 5.0
T10 4.7
T15 4.2
T4 3.7
T129 2.0
T53 0.9
S57 0.8
HadA
T118 1.2
Mycolic acid condensation, transport and transfer
AccD5
S8* 8.1
T2* 7.2
T29* 6.2
T18 4.3
MmpL3
T920 7.1
T984* 7.0
T979 1.1
T869 1.1
T923 -0.7
T840 -1.1
T946 -1.2
FadD32
S373* 6.2
T568* 4.4
T545* 3.1
AccA3
T533* 5.9
T310 3.6
Pks13
T1445* 3.7
T1450* 3.6
T14* 3.3
log2-transformed MS signal
20
25
30

Figure 5

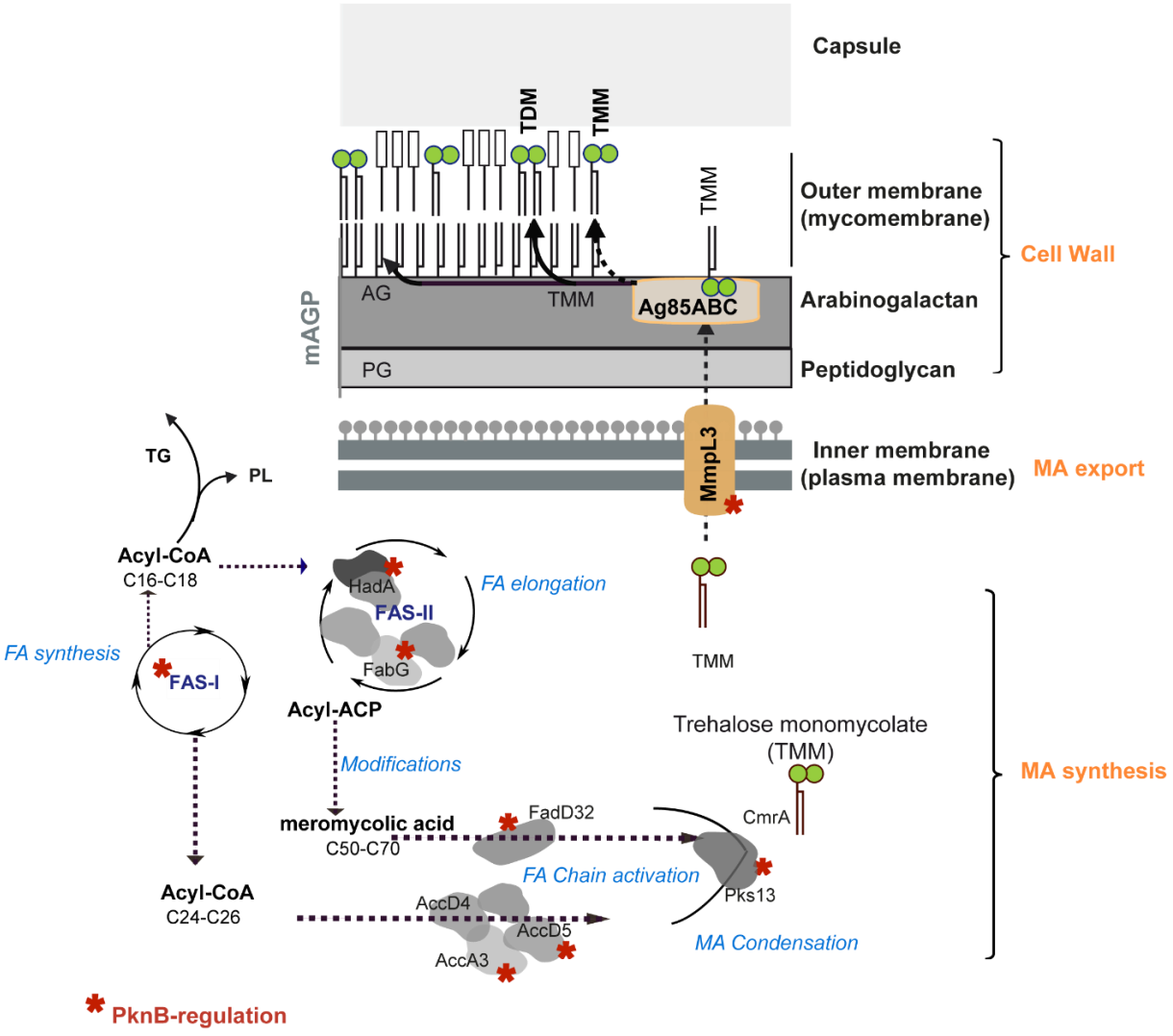
Capsule
TDM
TMM
TMM
Outer membrane
(mycomembrane)
Cell Wall
AG
TMM
Ag85ABC
Arabinogalactan
mAGP
PG
Peptidoglycan
MmpL3
Inner membrane
(plasma membrane)
MA export
TG
PL
Acyl-CoA
C16-C18
HadA
FAS-II
FA elongation
FabG
FA synthesis
FAS-I
Acyl-ACP
TMM
Trehalose monomycolate
(TMM)
Modifications
MA synthesis
meromycolic acid
C50-C70
FadD32
CmrA
FA Chain activation
Pks13
Acyl-CoA
C24-C26
AccD4
AccD5
AccA3
MA Condensation
PknB-regulation

FIGURE LEGENDS

Fig. 1. Depletion of PstP in *M. smegmatis* affects mycolic acid content. (**A**) Immunoblot analysis showing depletion of PstP in *Msm* mc²-cd-pstP cultures, grown in the absence (PstP+) or presence of ATc (PstP-) for 12h. Whole cell lysates of each culture were obtained, resolved on SDS-PAGE, transferred to nitrocellulose membrane and probed with anti-FLAG antibodies HRP-conjugates. (**B**) HPTLC profile of Total Extractable Lipids (TEL) of both strains obtained following CHCl3/CH3OH extraction, as described in Experimental Procedures. 75µg of TEL of each condition were loaded, and plate was developed with CHCl3/CH3OH/H2O (30/8/1 v/v) as solvent system and stained with primuline, then revealed with Chemidoc Imaging System. (**C**) Quantification of trehalose monomycolate (TMM) was performed using ImageLab (BioRad). Data are means ± SD of three independent replicates, *p*-values were calculated with Student's t-test (GraphPad Prism); ** $p \leq 0.01$. M: molecular marker.

Fig. 2. **Overexpression of PknB affects *M. smegmatis* growth and enhances mycobacterial susceptibility to large antibiotics.** (**A**) *In vitro* growth curves upon induction of PknB or PknB_K40M expression. Planktonic growth was established at 37 °C in 7H9-based medium supplemented with Tyloxapol and monitored as described in Experimental Procedures. All cultures were inoculated at an initial OD600 of 0.02 then IPTG-induced at OD600 of 0.6. Growth curves are represented in semi-logarithmic scale. Data are means ± SD of three independent experiments. The insert zooms on the PknB-dependent growth reduction indicated by an arrow. **(B)** Staining (Instant Blue) and immunoblot (anti-PknB antibodies) analysis to control PknB and PknB_K40M overproduction in *M. smegmatis*. Whole-cell lysates were obtained from pellets harvested at 4h post-induction, fractionated by SDS-PAGE and revealed as indicated. (**C)** Dose-inhibition curves of *M. smegmatis* overexpressing empty vector ("Control"), PknB or PknB_K40M in the presence of Vancomycin (VAN), rifampicin (RIF), isoniazid (INH) and ethambutol (EMB). Data are means ± SD of three independent experiments. The calculated (GraphPad Prism) IC50 (half inhibitory concentrations) for the different antibiotics are presented in panel (**D**).

Fig. 3. **PknB kinase activity impacts production of cell wall mycolic acids.** Radio-TLC profiles of whole cell fatty acids (**A**) and total extractable lipids (**B**) in *M. smegmatis* overexpressing the void vector (Control), PknB or PknB_K40M (K40M). Cultures were radio-labeled at 3h post-induction for 1h. (**A**) Radio-labeled fatty acids were saponified and extracted as described in Experimental Procedures. Same amounts of radio-labeled lipid extract of each strain were loaded onto a TLC plate developed with CH_2Cl_2. The quantification data (in arbitrary units AU) of total FAs (A1) and MAs (A2) (alpha (α), alpha prime (α') and epoxy (ep)) in the three strains are presented. **(B**) Radio-labeled TLE were extracted using $CHCl_3/CH_3OH$ as described in Experimental Procedures, loaded onto a TLC plate developed with $CHCl_3/CH_3OH/H_2O$ (30/8/1 v/v/v). Spots were revealed and quantified with PhosphoImager: trehalose dimycolate TDM (B1), trehalose monomycolate TMM (B2). triglycerides TG, glypeptidolipids GPLs, phospatidylethaloamine (PE), phosphotidylglycerol (PG), phosphotidylinositol (PI), phosphatidylinositol mannosides (PIM). The figure is representative of three independent experiments. Data are means ± SD of three replicates, *p*-values were calculated with Student's t-test (GraphPad Prism). *p≤ 0.05, ** $p \leq 0.01$, ****p<0.001.

Fig. 4. Label-free quantitative analysis of PknB-dependent phosphoproteome in *M. smegmatis*. (A) Schematic workflow of sample preparation and data analysis. Three independent cultures of *Msm* transformed with empty vector, *pknB*- or *pknB_K40M*-expressing vectors were prepared. Bacteria were lysed, proteins were trypsin-digested and phospho-containing peptides (pSTY) were then enriched using titanium dioxide (TiO_2) beads. Peptides before and after phospho-enrichment were analyzed by LC-MS/MS to determine the protein and phosphorylation site relative quantities across samples, respectively. Phosphorylation site relative quantities were normalized using their cognate protein relative quantities in order to correct for variations in protein expression across conditions. The normalized data were then subjected to statistical analysis to determine PknB-dependent phosphorylation events. **(B)** Heatmap of log2-transformed MS signal obtained for phosphorylation sites of interest across the 3 triplicate samples. The log2-transformed fold changes (PknB *Vs* PknB_K40M) are represented with the horizontal bar plot on the right-hand side. Fold changes in red highlight the phosphorylation sites that passed our statistical thresholds

(PknB *Vs* PknB_K40M, corrected p-value of two-sided unpaired Welch t-test ≤ 0.05 and minimum 2-fold change). Missing values are in grey.

Fig. 5. **Proposed model of cell wall remodeling by multistep STPK-regulation of mycolic acid biogenesis**. Phosphorylation of the mycobacterial *de novo* fatty acid synthase FAS-I would lead to reduced production of acyl-CoA pools, precursors of different lipids including triacylglycerol, phospholipids and mycolic acids. For mycolic acid synthesis, proteins of the FAS-II-mediated fatty acid elongation, chain activation (FadD32, AccA3/AccD5) and mycolic acid condensation (Pks13) to yield (after reduction by CmrA) trehalose monomycolate (TMM) are phosphorylated by PknB, resulting in decreased MA synthesis. Phosphorylation of MpmL3 impairs its TMM export to the outer membrane, leading to cytoplasmic TMM accumulation and severe decrease in TDM. TMM, the mycoloyl donor, is transferred by the mycoloyltransferases (Ag85 complex) to the biologically active mycolate-containing compounds (TDM, glucose monomycolates, glycerol monomycolates), as well as to arabinogalactan to form the mAGP complex. The negative control of key enzymes in MA biogenesis pathway, in addition to modulation of TMM amounts, result in overall cell wall remodeling. Red asterisks: PknB-regulated proteins identified and/or confirmed in this study.